

IMAGE RESTORATION USING NON-CIRCULANT SHIFT-INVARIANT SYSTEM MODELS

Antonios Matakos, Sathish Ramani, and Jeffrey A. Fessler

The University of Michigan
Department of Electrical Engineering and Computer Science
1301 Beal Avenue, Ann Arbor, MI 48109-2122

ABSTRACT

Image restoration is a well studied problem and there are several proposed methods for deblurring and denoising. Recently, there is increasing interest in iterative schemes that employ non-quadratic regularizers, especially edge-preserving like Total Variation (TV) and sparsity promoting like l_1 regularization. Most methods make simplifying assumptions concerning the system model and the most common one is the use of a circulant blurring model because it facilitates using the FFT. In this work we focus on a more realistic non-circulant blurring model and apply existing algorithms for image restoration with non-quadratic regularization, tailored to work with our non-circulant model.

Index Terms— Image restoration, Non-Circulant System, Edge-preserving Regularization

1. INTRODUCTION

In image restoration problems the goal is usually to reduce the effects of blurring and/or suppress noise. A naive deblurring method that simply inverts the blurring kernel can lead to severe noise amplification that degrades image quality. To achieve both goals (namely denoising and deblurring) several regularized image restoration methods have been proposed that take advantage of non-quadratic regularizers (like l_1 norm of wavelet coefficients [1, 2] or Total-Variation [3–5]) that suppress noise while preserving edges in the image. Most of these methods assume a circulant blur (periodic convolution with a blurring kernel), which even though accurate within the image, can lead to wraparound artifacts in the boundaries of the image due to the implied periodicity of the circulant model. Using a non-circulant model could prevent these artifacts at the cost of increased computational complexity.

In this work we propose to use a circulant blur model combined with a masking operator that prevents wraparound artifacts. Our proposed model is equivalent to the model used in [6], but in this work we focus on edge-preserving regularizers instead of the quadratic regularizer used in [6]. In addition our approach leads to a more elegant formulation that requires no pre-processing of the data or explicit treatment of the unknown, extrapolated boundaries [6]. The resulting model is non-circulant, but existing methods, like non-linear conjugate gradient (NCG), iterative shrinkage/thresholding (ISTA) [1, 7, 8], (M)FISTA [8], and Bregman splitting/Augmented Lagrangian (AL) [9–12], can be tailored for use in this case. All these methods can be applied to a general class of regularizers including edge-preserving (e.g., total-variation) and sparsity promoting (e.g., l_1 norm) regularizers that are commonly used in image restoration problems. Simulation results show that using the proposed non-circulant model leads to improved image quality at the boundaries where the commonly used circulant model is inaccurate.

2. PROBLEM FORMULATION

To design a restoration algorithm one must make some modeling assumptions. Often deblurring algorithms are developed assuming a circulant blur model represented by \mathbf{A} and the blurred and noisy image is modeled by:

$$\mathbf{y} = \mathbf{A}\mathbf{x} + \mathbf{n}, \quad (1)$$

where \mathbf{y} is the $(N \times 1)$ vectorized blurred and noisy image, \mathbf{n} is a $(N \times 1)$ zero-mean Gaussian noise vector, \mathbf{x} is the vectorized $(N \times 1)$ image to be reconstructed, and \mathbf{A} is a $(N \times N)$ circulant blurring matrix. Even though this model is very popular in the image restoration literature [1, 2, 5, 10, 13–16], it is inaccurate since the assumption of circulant blur rarely, if ever, applies in practice.

Reconstructing images under the assumption of a purely circulant model can lead to severe artifacts due to the discontinuities at the boundaries caused by the periodic extension of the image [6]. Simple approaches like zero-padding or boundary extension do not resolve this issue since they do not eliminate the discontinuity at the boundaries. As suggested in [6] data pre-processing techniques like boundary extension combined with edge-tapering can reduce, but not completely eliminate the reconstruction artifacts. This will be illustrated in the experiments section (§4).

For some practical applications it may be reasonable to assume the blur is shift-invariant inside the region of interest, but it is not pragmatic to consider that acquired data originated from a blurring system with periodic end conditions. In reality, there is not enough information about the blur at the boundaries of the image, so for reconstruction purposes, it is more practical to use a non-circulant model.

In this work, similarly to [6], we consider a more realistic non-circulant model, avoiding the assumption of periodic end conditions, by introducing a masking operator that eliminates the wraparound artifacts at the boundaries caused by periodic convolution. We consider the following model:

$$\mathbf{y} = \mathbf{T}\mathbf{A}\mathbf{x} + \mathbf{n}, \quad (2)$$

where \mathbf{y} is the vectorized blurred and noisy $(M \times 1)$ image, \mathbf{n} is a $(M \times 1)$ zero-mean Gaussian noise vector, \mathbf{x} is the vectorized $(N \times 1)$ image to be reconstructed with $N > M$, \mathbf{A} is a $(N \times N)$ circulant blurring operator, and \mathbf{T} is the $(M \times N)$ masking operator that truncates the circular wraparound at the boundaries. Even though the model in (2) is shift-invariant within the image, the use of the masking operator makes the overall system model $\mathbf{T}\mathbf{A}$ shift-variant.

Regularized image restoration can be approached in two main ways. One is the analysis formulation [17], where the objective is to obtain an estimate of the true image $\hat{\mathbf{x}}$, and the other is the synthesis formulation [1], where the objective is to estimate a set of transform

coefficients $\hat{\mathbf{w}}$ and obtain the reconstructed image through a transform as $\hat{\mathbf{x}} = \mathbf{W}'\hat{\mathbf{w}}$.

2.1. Analysis Formulation

Our goal is to estimate the image \mathbf{x} by minimizing the following cost function that we call problem **P0**:

$$\hat{\mathbf{x}} = \underset{\mathbf{x}}{\operatorname{argmin}} \left\{ \Psi(\mathbf{x}) \triangleq \frac{1}{2} \|\mathbf{y} - \mathbf{TA}\mathbf{x}\|_2^2 + \lambda\Phi(\mathbf{R}\mathbf{x}) \right\}, \quad (3)$$

where Φ is a regularizer function, \mathbf{R} is a sparsifying transform (*e.g.*, wavelet or finite differences) and λ is the regularization parameter.

The cost function Ψ in (3) can accommodate a general class of regularizers, but for the purpose of this work we will focus on edge-preserving and sparsity promoting regularizers like Total Variation (TV) and l_1 regularization, respectively.

1. l_1 regularization or discrete anisotropic total-variation:

$$\Phi(\mathbf{R}\mathbf{x}) = \|\mathbf{R}\mathbf{x}\|_1, \quad (4)$$

where $\mathbf{R} = \mathbf{W}$ is a wavelet frame or $\mathbf{R} = \mathbf{C} \triangleq [\mathbf{C}'_1 \ \mathbf{C}'_2]'$ is a matrix of horizontal and vertical finite differences.

2. Discrete isotropic total-variation

$$\Phi(\mathbf{C}\mathbf{x}) = \sum_{n=1}^N \sqrt{|\mathbf{C}_1\mathbf{x}|_n|^2 + |\mathbf{C}_2\mathbf{x}|_n|^2}. \quad (5)$$

The minimization of (3) is a non-trivial optimization problem. There are several proposed methods that could be used for this task, like NCG, ISTA, MFISTA and Bregman Splitting/AL that will be discussed in §3.

2.2. Synthesis Formulation

For the synthesis formulation we used a wavelet frame as the sparsifying transform \mathbf{W} , and l_1 norm of the wavelet coefficients as the sparsity promoting regularizer. The cost function is minimized over the wavelet coefficients \mathbf{w} and the restored image is then given by $\hat{\mathbf{x}} = \mathbf{W}'\hat{\mathbf{w}}$. In this case, the original problem **P0** is expressed as:

$$\hat{\mathbf{w}} = \underset{\mathbf{w}}{\operatorname{argmin}} \left\{ \Psi(\mathbf{w}) \triangleq \frac{1}{2} \|\mathbf{y} - \mathbf{TAW}'\mathbf{w}\|_2^2 + \lambda\|\mathbf{w}\|_1 \right\}, \quad (6)$$

where λ is the regularization parameter. Similar methods as those used for the analysis formulation can also be used to solve this problem.

3. METHODS

To solve the optimization problem **P0** we could use any of the available methods tailored to our proposed non-circulant model. **NCG** requires the use of a rounding parameter to approximate the non-differentiable absolute value function and thus, will not converge to an exact solution of **P0**. Also, even with an efficient line search method [18], it may still converge slowly and be computationally expensive. On the other hand **AL** methods like **SALSA** [10] could converge to an exact solution of **P0**, but for the non-circulant model the inner updates are not exact and it would require the use of CG for solving the inner sub-problems that may lead to increased computation time. In this work, since convergence speed is not our focus, we chose to use **MFISTA** for several reasons. First it converges faster than the simpler **ISTA** and unlike **NCG** it converges to a solution of

P0. Also compared to **SALSA** it is easier to implement and does not require CG iterations or any parameter tuning to ensure quick convergence.

For the synthesis formulation all steps of **MFISTA** are exact, and the only parameter to consider is a constant L , which is an upper bound on the Lipschitz constant of $\nabla f(\mathbf{w})$, where $f(\mathbf{w}) \triangleq \frac{1}{2} \|\mathbf{y} - \mathbf{TAW}'\mathbf{w}\|_2^2$. For our image restoration problem, the Lipschitz constant is $\max\operatorname{eig}(\mathbf{WA}'\mathbf{T}'\mathbf{TAW}')$ [8] and we can choose $L = \max\operatorname{eig}(\mathbf{A}'\mathbf{A}) = 1$, since we scale the blurring operator \mathbf{A} such that $\max\operatorname{eig}(\mathbf{A}'\mathbf{A}) = 1$, and $\mathbf{W}'\mathbf{W} = \mathbf{I}$ when \mathbf{W} is a tight frame, which gives:

$$\begin{aligned} \max\operatorname{eig}(\mathbf{A}'\mathbf{A}) &= \max\operatorname{eig}(\mathbf{AW}'\mathbf{WA}') = \max\operatorname{eig}(\mathbf{WA}'\mathbf{AW}') \\ &\geq \max\operatorname{eig}(\mathbf{WA}'\mathbf{T}'\mathbf{TAW}'). \end{aligned}$$

For the analysis formulation the minimization step in **MFISTA** in [8, Eq. (3.14)] cannot be performed exactly, but we can use a few iterations of a Chambolle-type algorithm as in [13, Eq. (6)–(7)] to find an approximate minimizer. Again, as in the synthesis formulation, we need to consider the parameter L which is an upper bound on the Lipschitz constant of $\nabla f(\mathbf{x})$, where $f(\mathbf{x}) \triangleq \|\mathbf{y} - \mathbf{Ax}\|$, and similarly to the synthesis formulation, we can choose $L = \max\operatorname{eig}(\mathbf{A}'\mathbf{A}) = 1$. For the inner Chambolle-type iterations we also need to consider another parameter $c \geq \max\operatorname{eig}(\mathbf{R}\mathbf{R}')$ [13, Eq. (6) and §A.2], where we can choose $c = 1$ for the wavelet l_1 norm regularizer, since $\max\operatorname{eig}(\mathbf{W}'\mathbf{W}) \leq 1$ when \mathbf{W} is a frame, and $c = 8$ for the TV regularizer since $\max\operatorname{eig}(\mathbf{C}'\mathbf{C}) = 8$.

4. EXPERIMENTS

For all our experiments we used the 256×256 cameraman image as the true, noise-free image, and following the experimental setting in [14] we scaled it to the range $[0, 1]$ (Figure 1). For the blurring kernel we used a uniform 9×9 blur. For this image and blur size the valid part of the convolution is the 248×248 central region and the data created with Matlab's `conv2` function using the `'valid'` option are of this size.

To assess the quality of our proposed non-circulant reconstruction method we compared it to reconstructions from a purely circulant model (no data pre-processing) and reconstructions where we used boundary replication combined with edge tapering, as pre-processing steps, before reconstructing with a purely circulant model. When using the non-circulant model in (2) or the unrealistic circulant model in (1) with data pre-processing the reconstructed images have original 256×256 size and then they are truncated to match the data size. When reconstructing with the unrealistic circulant model in (1) without pre-processing, the reconstructed image has the same size as the data, so no truncation is necessary.

For the analysis formulation, we used three types of regularizers, namely isotropic and anisotropic Total Variation, and l_1 norm of the coefficients of the undecimated 2-level Haar wavelet transform, excluding the approximation level. For the synthesis formulation, we used the l_1 norm of the coefficients of the undecimated 2-level Haar wavelet transform, including the approximation level.

We performed three sets of experiments with different levels of BSNR. We chose the regularization parameter λ to achieve low NRMS error and an aesthetically pleasing output image for a given BSNR level. The experiments we performed are as follows

1. 30 dB BSNR ($\sigma^2 = 5.03 \times 10^{-5}$) with $\lambda = 2^{-12}$,
2. 40 dB BSNR ($\sigma^2 = 5.03 \times 10^{-6}$) with $\lambda = 2^{-15}$,
3. 50 dB BSNR ($\sigma^2 = 5.03 \times 10^{-7}$) with $\lambda = 2^{-17}$,



Fig. 1. Cameraman true image (248×248), scaled to the range $[0, 1]$.

where σ^2 is the Gaussian noise variance. We quantified the reconstruction quality by computing the ISNR between the restored image $\hat{\mathbf{x}}$ and the true image \mathbf{x}_{true} . The ISNR was measured in the 248×248 central region that corresponds to the valid part of the convolution, since this was the actual size of the input data vector \mathbf{y} . Any extrapolated values are not used in the ISNR calculations and not shown in any of the figures.

Figure 2 shows the restored images from experiment 2 (40db BSNR) for the analysis formulation using isotropic TV regularization, and for the synthesis formulation using wavelet l_1 norm regularization. As we see in Fig. 2b and 2f the restored images using the unrealistic circulant model in (1) exhibit severe ringing artifacts that are not only contained around the edges of the image. When data pre-processing is used the ringing artifacts are significantly reduced, but not completely removed (Fig. 2c and 2g). These artifacts can be more severe and lead to more degradation when the strength of the regularizer decreases as seen in the quantitative results in Table 1. Finally, we see that the reconstructed images from the proposed non-circulant model are free of any ringing artifacts and the quality of the reconstructed images closely resembles the true noise-free image (Fig. 2d and 2h).

Table 1 gives the quantitative results in terms ISNR for all experiments. In all cases the ISNR of reconstructions based on the non-circulant model are higher than that of the reconstructions based on the unrealistic circulant model without data pre-processing. In the case of reconstruction with the circulant model and data pre-processing we can see that for lower SNR, where stronger regularization is required, the smoothing of the regularizer can suppress the ringing artifacts leading to reconstruction ISNR comparable to the proposed non-circulant model reconstruction. However, in higher SNR regimes, where less smoothing is required, the artifacts from the circulant model reconstruction become more prominent and the non-circulant reconstruction shows significantly improved reconstruction quality.

5. DISCUSSION

As seen from the results section, reconstructing with an unrealistic circulant model can lead to severe distortion of the restored images. The ringing artifacts due to the discontinuity at the boundaries are not localized and even existing methods for data-preprocessing [6] cannot fully suppress these artifacts.

In conclusion, the proposed method showed significant improvement of the restored images, compared to the standard method that uses an unrealistic circulant reconstruction model. This illustrates the importance of using more realistic reconstruction models and also shows that the effects of model mismatch, even though commonly not accounted for, can be severe in terms of image quality

degradation. In addition the formulation of our model, even though similar to the one used in [6], leads to a more elegant approach of the non-circulant reconstruction problem that does not require any data pre-processing and estimation of the extrapolated image boundaries.

Finally, the existing reconstruction algorithms, even though they can be tuned for use with the non-circulant model, may converge slowly or can be very computationally intensive. For this purpose we have developed a new algorithm [19] based on the Augmented Lagrangian framework like the ones presented in [11, 12]. Our algorithm benefits from the fast convergence of AL methods, but avoids the computationally intensive inner minimizations of algorithms like SALSA [10].

6. REFERENCES

- [1] M. A. T. Figueiredo and R. D. Nowak, "An EM algorithm for wavelet-based image restoration," *IEEE Trans. Im. Proc.*, vol. 12, no. 8, pp. 906–16, Aug. 2003.
- [2] C. Vonesch and M. Unser, "A fast multilevel algorithm for wavelet-regularized image restoration," *IEEE Trans. Im. Proc.*, vol. 18, no. 3, pp. 509–23, Mar. 2009.
- [3] L. I. Rudin, S. Osher, and E. Fatemi, "Nonlinear total variation based noise removal algorithm," *Physica D*, vol. 60, no. 1-4, pp. 259–68, Nov. 1992.
- [4] T. F. Chan, S. Osher, and J. Shen, "The digital TV filter and nonlinear denoising," *IEEE Trans. Im. Proc.*, vol. 10, no. 2, pp. 231–41, Feb. 2001.
- [5] J. P. Oliveira, J. M. Bioucas-Dias, and M. A. T. Figueiredo, "Adaptive total variation image deblurring: A majorization-minimization approach," *Signal Processing*, vol. 89, pp. 1683–93, 2009.
- [6] S. J. Reeves, "Fast image restoration without boundary artifacts," *IEEE Trans. Im. Proc.*, vol. 14, no. 10, pp. 1448–53, Oct. 2005.
- [7] I. Daubechies, M. Defrise, and C. D. Mol, "An iterative thresholding algorithm for linear inverse problems with a sparsity constraint," *Comm. Pure Appl. Math.*, vol. 57, no. 11, pp. 1413–57, Nov. 2004.
- [8] A. Beck and M. Teboulle, "Fast gradient-based algorithms for constrained total variation image denoising and deblurring problems," *IEEE Trans. Im. Proc.*, vol. 18, no. 11, pp. 2419–34, Nov. 2009.
- [9] T. Goldstein and S. Osher, "The split Bregman method for L1-regularized problems," *SIAM J. Imaging Sci.*, vol. 2, no. 2, pp. 323–43, 2009.
- [10] M. V. Afonso, José M Bioucas-Dias, and Mário A T Figueiredo, "Fast image recovery using variable splitting and constrained optimization," *IEEE Trans. Im. Proc.*, vol. 19, no. 9, pp. 2345–56, Sept. 2010.
- [11] S. Ramani and J. A. Fessler, "Parallel MR image reconstruction using augmented Lagrangian methods," *IEEE Trans. Med. Imag.*, vol. 30, no. 3, pp. 694–706, Mar. 2011.
- [12] S. Ramani and J. A. Fessler, "A splitting-based iterative algorithm for accelerated statistical X-ray CT reconstruction," *IEEE Trans. Med. Imag.*, vol. 31, no. 3, pp. 677–88, Mar. 2012.
- [13] I. W. Selesnick and Mário A T Figueiredo, "Signal restoration with overcomplete wavelet transforms: comparison of analysis and synthesis priors," in *Proc. SPIE Wavelets XIII*, 2009, p. 74460D, Wavelets XIII.
- [14] A. Beck and M. Teboulle, "A fast iterative shrinkage-thresholding algorithm for linear inverse problems," *SIAM J. Imaging Sci.*, vol. 2, no. 1, pp. 183–202, 2009.
- [15] M. A. T. Figueiredo and José M Bioucas-Dias, "Restoration of Poissonian images using alternating direction optimization," *IEEE Trans. Im. Proc.*, vol. 19, no. 12, pp. 3133–45, Dec. 2010.
- [16] M. V. Afonso, J. M. Bioucas-Dias, and M. A. T. Figueiredo, "An augmented Lagrangian approach to the constrained optimization formulation of imaging inverse problems," *IEEE Trans. Im. Proc.*, vol. 20, no. 3, pp. 681–695, 2011.

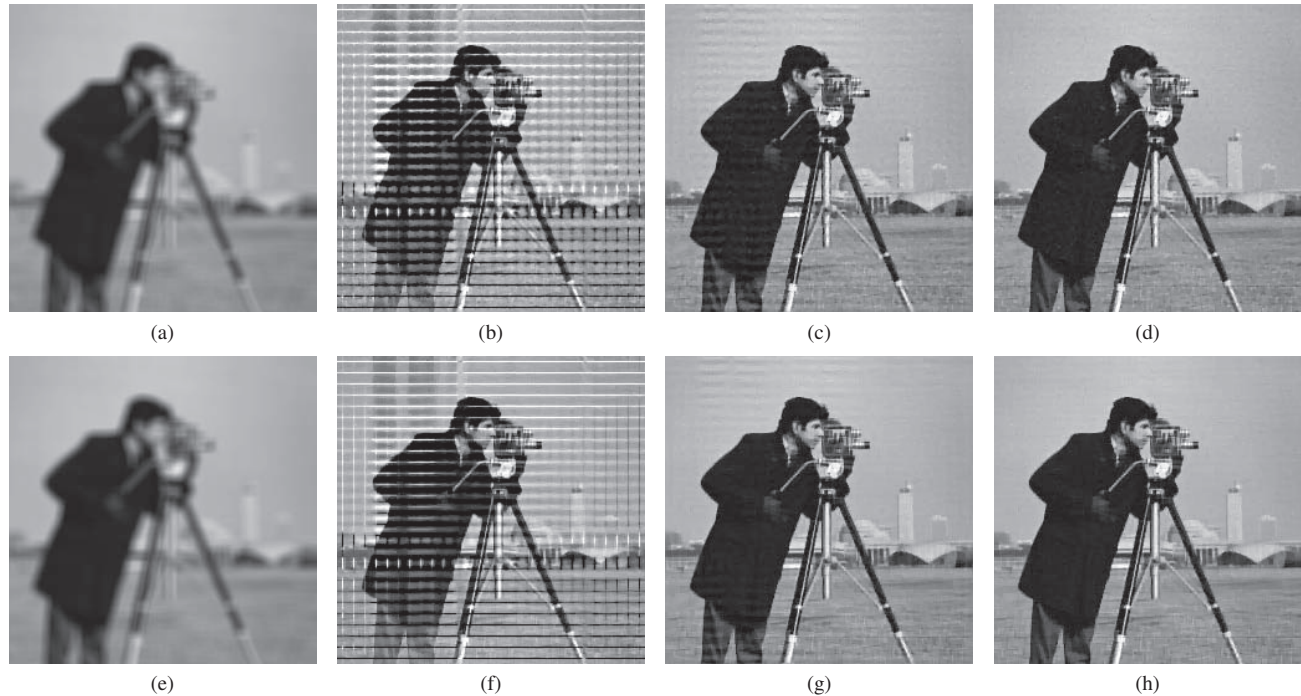


Fig. 2. Experiment 2: Restoration results for analysis formulation using isotropic TV regularization (first row) and for synthesis formulation using wavelet l_1 norm regularization (second row). (a,e) Blurred and noisy images from non-circulant model. (b,f) Restored images from unrealistic circulant model. (c,g) Restored images from unrealistic circulant model with data pre-processing. (d,h) Restored images from proposed non-circulant model

Table 1. ISNR in db for all experiments. The * denotes reconstruction using the unrealistic circulant model with data pre-processing.

Reg. Type	Experiment 1			Experiment 2			Experiment 3		
	Non-Circ.	Circ.	Circ.*	Non-Circ.	Circ.	Circ.*	Non-Circ.	Circ.	Circ.*
Analysis formulation									
Wavelet l_1	5.7	-3.3	5.6	8.6	-8.1	7.9	11.8	-10.5	9.0
TV _{ANISO}	5.6	-3.5	5.4	8.4	-8.4	7.5	12.0	-10.3	8.3
TV _{ISO}	5.7	-3.7	5.6	8.3	-8.6	7.3	11.6	-10.4	8.2
Synthesis formulation									
Wavelet l_1	5.7	-3.3	5.6	8.6	-8.1	7.9	11.8	-10.6	9.0

- [17] M. Elad, P. Milanfar, and R. Rubinstein, "Analysis versus synthesis in signal priors," *Inverse Prob.*, vol. 23, no. 3, pp. 947–68, June 2007.
- [18] J. A. Fessler and S. D. Booth, "Conjugate-gradient preconditioning methods for shift-variant PET image reconstruction," *IEEE Trans. Im. Proc.*, vol. 8, no. 5, pp. 688–99, May 1999.
- [19] A. Matakos, S. Ramani, and J. A. Fessler, "Image restoration using non-circulant system models," *IEEE Trans. Im. Proc.*, 2012, Submitted as TIP-08903-2012.